이학석사 학위논문

Future change of East Asian extratropical cyclones in CMIP5 models

CMIP5 모델에서 나타나는 미래 동아시아
온대저기압의 변화

2018년 8월

서울대학교 대학원

지구환경과학부

이 재 연

Abstract

Extratropical cyclones (ETCs) in East Asia are detected and tracked by applying an automated tracking algorithm to the 850-hPa relative vorticity field. The ETC statistics during the period of 1979-2014 show that East Asian ETCs primarily organize over Mongolia, South China, and the Kuroshio Currents. Both Mongolia and South China ETCs form on the leeward side of the mountains in these regions. Kuroshio ETCs develop in regions with a sharp SST gradient. The response of East Asian ETCs to anthropogenic forcing is also studied through a comparison of historical simulations and a RCP 8.5 scenario of CMIP5 models. Historical simulations reproduce spatial distribution and seasonality of ETC frequency, genesis, intensity, and growing rate qualitatively well. But, ETC genesis in the South China region is underestimated in quantity. The frequency and intensity of ETCs decrease in future scenarios particularly over the western North Pacific due to diminished cyclogenesis downstream of the Tibetan plateau and across the Kuroshio Current and due to vertical wind shear and static stability changes in the warming climate.

Table of Contents

1. Introduction

Extratropical cyclones (ETCs) are known to play an important role in a mid-latitude water cycle and their activity relates to about seventy percent of seasonal precipitation in some part of East Asia (Hawcraft et al., 2012). In addition, intense ETCs with wind storms and storm surges cause significant socio-economic damage (Fink et al., 2009). Due to these weather and climate impacts of ETCs, there are many efforts to understand East Asian ETCs.

Chung et al. (1976) reported that East Asian ETCs are mainly generated on the leeside of high mountains. Whittaker and Horn (1984) studied East Asian ETCs from 1958 to 1977 and reported that East Asian ETCs generally form over the ocean near Southern China and that these oceanic ETCs are more intense than continental ETCs. Chen et al. (1991) extended the result of Whittaker and Horn (1984) using the sea level pressure field. They classified the development of East Asian cyclones under cyclogenesis in the leeside of mountains (e.g. Altai-Sayan mountains and Tibetan Plateau) and over the ocean (e.g. the East Sea and the east coast of Japan). Trenberth (1991) defined storm tracks as the band pass filtered variability of the geopotential height at 500 hPa. The storm track was strongest at 50°S and this position was related to baroclinicity at lower troposphere and the peak of the jet stream.

Previous studies about East Asian ETCs manually tracked ETCs

1

through the use of daily weather maps or were based on case studies or short-term studies. However, manual ETC tracking is subjective and studies done over short periods do not show climatic features of ETCs. For these reasons, automated tracking algorithms are used in recent ETC studies. For instance, Raible (2007) showed that explosively deepening ETCs identified as local minima of the geopotential height at 1000 hPa were related to wintertime atmospheric circulations. Gulev et al. (2001) referred to a decadal variability of wintertime ETCs' climatic characteristics (e.g. ETC frequency, intensity, and growing rates) using the sea level pressure field. Hoskins and Hodges (2002) and Bengtsson et al. (2006) reported that ETCs in winter had the highest growing rates in the western boundary region of the ocean and that their genesis and lysis regions generally occurred on the border of high topography.

As it becomes available to use climate models which can simulate change of atmospheric circulation in future scenarios, the response of ETCs to global warming is highlighted because global warming has emerged with an increased carbon dioxide emission in recent years. But previous Coupled Model Intercomparison Project (CMIP) series is inadequate for an automated tracking algorithm, since all models do not provide data shorter than six hourly intervals which is needed for tracking ETCs. So a simple ETC identification technique (Lambert and Fyfe, 2006) and Eulerian variances in atmospheric synoptic waves

(Ulbrich et al., 2008) have been used for ETC studies. Lambert and Fyfe (2006) showed the total number of northern hemispheric ETCs decreased but the number of intense ETCs increased with enhanced greenhouse gas forcing. Ulbrich et al. (2008) identified enhanced baroclinic wave activity in the mid-latitudes from anthropogenic forcing.

As high-frequency (six hourly interval) model output data is included in CMIP5 (Taylor et al., 2012), multi-model experiments using automated tracking algorithms started. Colle et al. (2013) evaluated the performance of the top seven CMIP5 models in simulating North American ETC characteristics (e.g. track density and intensity). They suggested that ETC storm track density and ETC intensity would decrease over the western Atlantic in the future. Zappa et al. (2013) confirmed the result of Lambert and Fyfe (2006). They reported that the number of overall wintertime ETCs decreased but the number of explosive cyclones increased in the Northern Atlantic and in Europe. Zappa et al. (2014) found a reduction of Mediterranean ETCs under the Representative Concentration Pathway 8.5 (RCP 8.5) scenario.

Recently, there are some previous studies on the ETC responses to anthropogenic forcing in CMIP5 models using an automated tracking algorithm. However, these studies do not focus on future changes of East Asian ETCs. Though some studies can provide overall information about ETCs, they can overlook local processes which are important in

the development of ETCs. The formation and growth of ETCs are as affected by local forcings as global atmosphere circulation changes. In particular, complex topography and coastlines in East Asia can instigate strong local forcing. Other studies have analyzed ETCs in a more local perspective but mostly cover North Atlantic or Mediterranean ETCs.

The goal of this study is to analyze the response of East Asian ETCs to an increased greenhouse gas forcing. This paper is separated into three parts. First, the climatology and seasonality of East Asian ETCs is presented. Followed by the performance of CMIP5 models in analyzing East Asian ETCs. Based on these results, the future response of East Asian ETCs to the high emissions (RCP 8.5) scenario is discussed.

2. Data and Methods

2.1. Data

Models archived for CMIP5 are used at six hourly intervals. These models provide historical simulation and the RCP 8.5 scenario. The historical simulation is forced by observed atmospheric changes in the 20th century. The RCP 8.5 scenario is a future projection which incorporates the increase of radiative forcing under high emissions scenarios.

23 models which are used in this study are listed in Table 1. All models have different resolutions. As these different resolutions can cause uncertainty, all models are interpolated onto a resolution of 1.5 degrees of latitude and longitude. A multi-model mean is conducted using these interpolated model outputs. The European Centre for Medium-Range Weather Forecasts (ECMWF) Interim Re-Analysis (Dee et al., 2011) dataset is regarded as the reference point. For the comparison of the reanalysis data, the historical simulation during the 26-year period (1979-2004) is considered. RCP 8.5 simulation for the last 26 years (2074-2099) is used, just like the period for the historical simulation.

2.2. ETC detection and tracking

  In this study, ETC is defined on the relative vorticity field at 850

hPa. ETCs are normally identified through the sea level pressure field. But the East Asian continent has complex and broad mountains, leading to large errors in mountainous regions. Using 850 hPa variables can reduce this problem. The relative vorticity has an advantage over the sea level pressure as only well-developed low pressures in the sea level pressure field can be captured. When using the relative vorticity field, more ETCs are identified as early stage and small cyclones in addition to mature ones are included. Although the local maxima of the relative vorticity and local minima of the sea level pressure do not always coincide, those two variables show same qualitative results (Lee et al., 2016). The relative vorticity which is used in this study has a T42 spectral grid and from wave number 5 to 42. To focus on the synoptic scale, the relative vorticity is smoothed to the T42 grid in the spectral domain. Small wave numbers below five are filtered to remove the background vorticity field.

ETCs are tracked by using an automated tracking algorithm (Hodges, 1994, 1995, 1999). This tracking algorithm separates individual cyclones from the relative vorticity field. The center of an ETC, which is defined as the local maxima, is tracked through three consequtive time steps (t-1, t, t+1). ETC tracks are smoothed by using a cost function relating distance and direction (See Hodges (1994, 1995, 1999) for more information). Statistical analysis of ETCs are done

through an automated tracking algorithm.

2.3. ETC properties

In this paper, cyclone properties (e.g. ETC frequency, ETC intensity, cyclogenesis regions, and ETC growing rate) are defined to understand characteristics of East Asian ETCs. These properties are similar to those described in Plante et al. (2014). ETC frequency indicates the number of ETCs which can affect an area. The number of ETCs which traverse a given area is counted only once per month because double counting is biased towards slowly moving ETCs. ETC frequency are counted in a circular area with a 555 km radius of influence from a given grid point. This radius is reflective of the synoptic scale size of ETCs. The area of the circle with this radius does not biased to latitude at all grid points. ETC intensity (in CVU, Cyclonic Vorticity Units; 1.0×10^{-5} s^{-1}) is defined as the local maxima of the relative vorticity field at 850 hPa. The mean intensity at each grid point is the average of intensity of detected ETCs within a radius of influence. The cyclogenesis region indicates a first point of detected ETC track in a given area. This definition makes the cyclogenesis region sensitive to tracking parameters and the detection scheme. ETC growing rate is identified as the absolute value of the difference of ETC intensity over 6hours.

3. Results

3.1. Climatology of East Asian ETCs

Figure 1 shows the climatology of East Asian ETC characteristics over 36 years (1979-2014). The first two panels show ETC frequency (Fig. 1a) and ETC intensity (Fig. 1b). The other panels represent the growing rate (Fig. 1c) and cyclogenesis region (Fig. 1d).

ETC frequency is pronounced in three regions: West Siberia, Mongolia, and the Kuroshio Current. In these regions, six to seven ETCs are observed per month. It is consistent to the results of Zhang et al. (2012) who reported East Asian ETCs generally form in West Siberia, Mongolia, and over the coast near eastern China, then decay over Siberia north of 60°N, over Northeast China, and the Okhotsk Sea-northwest Pacific region.

Among these three regions, the highest ETC frequency is located over West Siberia. However, their intensity is not quite strong (Fig. 1b). As shown by Fig. 1c, the cyclogenesis map is quite small in West Siberia because ETCs passing through this region are mostly generated on the leeside of the Ural Mountains (Chen and Zhang, 1996). They grow slowly, travel fast over long distances toward Siberia and then decay at 80°E, and suggesting ETCs in West Siberia are mostly decaying ETCs.

East Asian ETCs are also prevalent over Mongolia. These ETCs, which are referred as Mongolia ETCs, are mainly generated downstream

of the Altai-Sayan mountains and develop rapidly (Figs. 1c, d). Figure 2a further shows the tracks of individual Mongolian ETCs. Here, the blue (red) shading indicates weak (strong) ETCs. Initial Mongolian ETCs develop slowly, traveling towards northeast China and the East Sea. Then they rapidly intensify over the ocean due to strong baroclinicity and abundant moisture supply (Hirata et al., 2015). Most Mongolian ETCs move eastward but the spread of their tracks is wide. Yellow dust events can occur in Korea when springtime Mongolia ETCs pass through the northeast region of the Korean peninsula (Lee et al., 2016).

Despite no distinct ETC frequency and intensity (Figs. 1a, b), there is a major East Asian cyclogenesis region in the leeside of the Tibetan Plateau (Fig. 1d). The tracks of these ETCs which are referred to as South China ETCs are illustrated in Fig. 2b. South China ETCs travel eastward or northeastward towards the Kuroshio Current region. They also grow rapidly over the ocean like Mongolian ETCs.

Figure 1a shows that ETC frequency is high in the Kuroshio-Oyashio Extension. The ETCs in this region, which are referred to as Kuroshio ETCs, form over the Kuroshio Current and develop rapidly in the baroclinic environment and with the abundance of diabatic heating (Hirata et al., 2015). Unlike most East Asian ETCs, which generally move along the jet stream, Kuroshio ETCs break through the jet stream while rapidly intensifiying as shown in Fig. 2c (Hayasaki and Kawamura, 2102;

Hayasaki et al 2013).

In short, developing East Asian ETCs are generated in the leeside of the Altai-Sayan mountains (Mongolia ETCs), the Tibetan Plateau (South China ETCs), and near the Kuroshio Current (Kuroshio ETCs). In particular, Continental ETCs (Mongolia ETCs and South China ETCs) generally develop slowly over the continents, and then grow rapidly over the ocean. All East Asian ETCs tend to decay rapidly in the western North Pacific where sea surface temperature is low (not shown).

3.2. Seasonality of East Asian ETCs

Figure 3 shows the seasonal cycle of ETC frequency, ETC intensity, and cyclogenesis region in East Asia. Although all seasonal features of ETCs in East Asia are similar to the annual climatology shown in Fig. 1a, b, and d, there are still noticeable differences between the seasons.

The seasonal distribution of ETC frequency is shown in the left panels of Fig. 3. The three maxima still exist but their exact locations across the seasons. The peaks of ETC frequency move equatorward from summer to winter along with an equatorward shift of the westerly jet.

The maxima of ETC frequency over the ocean and over the continent have a different seasonality from each other (compare DJF and JJA in Fig. 3). For example, oceanic ETCs (e.g., Kuroshio ETCs; box C)

have higher frequencies during all seasons except winter but continental ETC frequencies (e.g., Mongolia ETCs and South China ETCs) are the largest during the transition seasons (e.g., spring and fall). This seasonal change which is quantitatively shown in Fig. 4 is correspond to the findings of Lambert (1996) and Graham and Diaz (2001). Strong wintertime oceanic ETC activity is explained well by the seasonal march of local baroclinicity near the Kuroshio Current but the detailed mechanisms of the highest continental ETC frequency in the transition seasons are still not clear.

The middle column in Fig. 3 displays the seasonality of ETC intensity. There is a strong intensity over the Kuroshio-Oyashio Extension. In this area, ETC intensity is stronger in winter than in summer. It is similar with the seasonality of ETC frequency but with a noticeable difference. ETC intensity is the strongest in the spring for all ETCs over East Asia. The intensities of Mongolian and South China ETCs are approximately 3.0-3.3 CVU in spring, and their springtime intensities are about 15-27% (approximately 0.4-0.7 CVU) larger than the total winter ETC intensity (Figs. 4a, b). Kuroshio ETCs also show the largest intensity in spring. This seasonal variability is referred to by Nakamura (1992) as the midwinter suppression of the Pacific storm track and suggests that this seasonality of East Asian ETC intensity cannot be explained by linear baroclinicity alone.

Lastly, the seasonal distribution of East Asian cyclogenesis are shown in the right panels in Fig. 3. Throughout all seasons, the pattern of East Asian cyclogenesis are similar but with different frequencies. For instance, cyclogenesis over the Kuroshio Current is the maximum in winter (approximately two ETCs per month) and the minimum in summer (approximately one ETC per month) and the seasonal variation of continental cyclogenesis is the largest in spring (approximately two to four ETCs per month). These results resemble the seasonality of ETC frequency.

3.3. Simulation of CMIP5 models for East Asian ETCs

With understanding of climatological features, characteristics of East Asian ETCs in historical simulation of CMIP5 models are studied first. The result in sections 3.1 are used as the reference data for comparing with the model result calculated by the multi-model mean.

Figure 5 shows simulation of CMIP5 climate models for ETC frequency (first row), cyclogenesis region (second row), ETC intensity (third row) and growing rate (fourth row) in East Asia. There is a quantitative difference between the results of the historical simulation in middle column and that of the reference data (ERA-Interim reanalysis data) in the left column.

The differences of ETC frequency and cyclogenesis between

reanalysis data and historical simulation are shown in first and second rows of Fig. 5. In a cyclogenesis map, historical simulation quantitatively underestimates lee cyclogenesis near the downstream of the Altai-Sayan mountains and the Tibetan Plateau. The underestimated ETCs which are generated in the leeside of East Asian mountains affects the ETC frequency in historical simulations. East Asian ETCs are less frequent in historical simulations than when using reanalysis data. This difference is noticeable not only near the leeside of East Asian mountains but also over Kuroshio-Oyashio Extension. This difference is not related to the horizontal and vertical resolutions of CMIP5 models (not shown).

ETC intensity and growing rate in East Asia also have quantitative differences between reanalysis data and historical simulation (see third and fourth rows of Fig. 5). The difference in growing rate map corresponds to that in the cyclogenesis map which underestimates the number of cyclogenesis near the leeside of East Asian mountains (e.g., the Altai-Sayan mountains and the Tibetan Plateau) and over the Kuroshio-Oyashio Extension. East Asian ETC intensity in historical simulation is also underestimated over the Kuroshio-Oyashio Extension and is about 0.5 CVU smaller than that in the reanalysis data.

Despite these quantitative underestimations of East Asian ETC features, historical simulation qualitatively simulates East Asia ETCs

well. Historical simulation of CMIP5 climate models well captures the three peaks of ETC frequency (e.g., the locations in West Siberia, Mongolia, and the Kuroshio Current). Cyclogenesis is also qualitatively well simulated the three major cyclogenesis regions (e.g., the locations in the leeside of the Altai-Sayan mountains, the Tibetan Plateau, and near the Kuroshio Current). In short, historical simulation of CMIP5 climate models underestimates but qualitatively simulates well for the characteristics of East Asian ETCs.

3.4. The change of East Asian ETCs in RCP 8.5 scenario

3.4.1 Future change of climatic ETC features in East Asia

Based on the discussion in section 3.3, the response of East Asian ETCs to an increase of anthropogenic forcing is studied by a comparison (right panels of Fig. 6) between historical simulation (left panels of Fig. 6) and high emission scenario (RCP 8.5 scenario; middle panels of Fig. 6).

Figure 6 shows future changes of ETC frequency (first row) and cyclogenesis region (second row) in East Asia. East Asian ETCs in the RCP 8.5 scenario become less frequent than in historical simulation. This reduction of East Asian ETC frequency is noticeable near South China and the Kuroshio Currents (at 20-40°N). This decreased ETC frequency in high emission scenario is approximately 25% of total ETC

frequency (three ETCs per month) in historical simulation. Because this region is one of the major trajectories of South China ETCs, some of the reduction of ETC frequency in the future seem to be related to a change of cyclogenesis in the leeside of the Tibetan Plateau, the genesis region of South China ETCs. Cyclogenesis in the RCP 8.5 scenario declines near the South China region and implies a decrease of South China ETCs.

The third and fourth rows of Fig. 6 present the response of ETC intensity and growing rate to anthropogenic forcing. East Asian ETC intensity weakens in the RCP 8.5 scenario. Diminished ETC intensity in the future is mainly over the western North Pacific and is approximately 0.4 CVU less compared to the historical simulation. Growing rates of East Asian ETCs also decrease over the Kuroshio Currents. This decreased ETC growing rates are slightly located in lower latitudes than the peak of growing rates of East Asian ETCs. The reduction of ETC growing rates might be related to the diminished moisture supply, but more research is necessary to prove this connection.

To recap briefly, the number of East Asian ETCs decreases and weakens in the RCP 8.5 scenario and is related to a reduction of genesis and growing rates of East Asian ETCs.

To understand the response of East Asian ETC features to anthropogenic forcing, the Eady growth rate (Eady, 1949) is used to explain the baroclinic development of ETCs. This property is generally

used to explain zonal-mean flows and is based on linear wave dynamics. Nevertheless, it is still useful for understanding a change of weather systems. Here, the Eady growth rate is defined as

$$\sigma = 0.31\, f\, |\partial u/\partial z| N^{-1},$$

where f represents the Coriolis parameter, u the zonal wind, and N indicates the Brunt-Väisälä frequency. The zonal wind and the potential temperature at the 500- (or 250-) and 850-hPa pressure levels are used to calculate the Eady growth rate. The Eady growth rate consists of vertical zonal wind shear ($\partial u/\partial z$) and static stability (N). Vertical zonal wind shear is positively correlated with the development of ETCs and static stability is the opposite: it has a negative correlation to the growth of ETCs.

Figure 7 shows the change of dynamic variables (e.g., vertical zonal wind shear and static stability) in the RCP 8.5 scenario. Many previous studies are used to analyze the jet stream at 250-300 hPa or the eddy driven jet at 850 hPa to understand the atmospheric circulation change in future climates. Therefore, both upper-level and lower-level dynamic variables are considered in Fig. 7. Upper-level dynamic variables are calculated using atmospheric variables (e.g., the zonal wind and the potential temperature) at 250- and 850-hPa pressure levels and lower-level dynamic variables are computed using 500- and 850-hPa atmospheric variables.

Future change of upper-level static stability which involves the change of the upper-level potential temperature is insignificant in the mid-latitudes. It is the reason that the tropopause heights, which are simulated by CMIP5 climate models, are different from each other. However, given the uncertainty of each model, a change of upper-level static stability seems have no effect on East Asian ETCs in the RCP 8.5 scenario. There is a decreased upper-level vertical zonal wind shear in the location where South China ETCs pass through but it is not significant. Upper-level vertical zonal wind shear increases near Mongolia where Mongolia ETCs exist but this enhancement is cancelled by a declining upper-level static stability in this region.

The reduced and weakened East Asian ETCs can be explained through dynamic variables related to a low level baroclinicity rather than upper-level variables. Especially, the area where lower-level vertical zonal wind shear diminishes is quite similar to the distribution of a decreased ETC frequency in the RCP 8.5 scenario. Lower-level Static stability in the future also enhances over the whole domain of East Asia. To sum up, the reduction of East Asian ETC activity in the future scenario could be related with an increased lower-level vertical zonal wind shear and a decreased static stability.

3.4.2. Seasonality of future change of East Asian ETCs

Figure 8 presents a seasonal variation of future change of ETC frequency (top), vertical zonal wind shear (middle), and static stability (bottom). These results are computed by an averaged latitudinal blue box in Fig. 5. Throughout all seasons, East Asian ETCs decrease in the RCP 8.5 scenario and is noticeable in autumn season (from August to October). A seasonal variation of a reduction of ETC frequency corresponds to that of an increased static stability in the future scenario and vertical zonal wind shear also declines during the autumn season. The seasonal variability of a reduction of East Asian ETC frequency in the RCP 8.5 scenario seems to be contributed by the seasonal variation of static stability in all seasons except autumn. The reduction of fall East Asian ETC frequency seems to be influenced by a change of vertical zonal wind shear and static stability in the future scenario.

Figure 9 shows the scatterplot which illustrates the relationships between future changes of ETC frequency and dynamic variables (e.g., vertical zonal wind shear and static stability) in the individual CMIP5 models. Each scatterplot in Fig. 9 represent the results in all seasons (left), winter (middle), and summer (right). Transient seasons (e.g., spring and autumn) are not considered.

Both changes of static stability and vertical zonal wind shear show a significant correlation of change of annual East Asian ETC frequency in the RCP 8.5 scenario. Most CMIP5 models present the increased static

stability and the diminished vertical zonal wind shear with the decline of ETC frequency in the RCP 8.5 scenario. However, some models (e.g., MPI-ESM-MR, MPI-ESM-LR, and GFDL-ESM2M) show increased vertical zonal wind shear. In addition, the change of vertical zonal wind shear have wider intermodel spread than that of static stability. The changes of wintertime ETC frequency are significantly correlated with only that of static stability. Vertical zonal wind shears of the individual models in winter do not change systematically. The reduction of wintertime ETC frequency cannot be understood in linear baroclinicity but the decreased ETC frequency in summer can. Summertime ETCs change with two dynamic variables. All models show the enhanced static stability and the diminished vertical zonal wind shear with the reduction of ETC frequency in high emission scenario except the bcc-csm1-1-m model.

4. Summary and Discussion

This paper studied the response of East Asian ETCs to anthropogenic forcing based on the understanding of climatic and seasonal features of ETCs in East Asia using an automated tracking algorithm. In reanalysis data, there are the three peaks of ETC frequency in West Siberia, Mongolia, and the Kuroshio Currents. ETCs in West Siberia are generated in the leeside of the Ural Mountains and travel toward western Siberia plain while weakening. ETCs in Mongolia mainly consist of developing ETCs and form through lee cyclogenesis in the leeside of the Altai-Sayan mountains. ETCs near the Kuroshio Currents consist of South China ETCs which are generated from the leeside of the Tibetan Plateau and Kuroshio ETCs which develop over the Kuroshio-Oyashio Extension.

East Asian ETC frequency is underestimated in the historical simulation of CMIP5 models. It is related to the underestimation of cyclogenesis in the leeside of the Altai-Sayan mountains and the Tibetan Plateau. CMIP5 models show that ETC intensity and growing rates weaken near Kuroshio-Oyashio Extension where East Asian ETCs develop rapidly. Despite this underestimation, CMIP5 climate models well capture the distribution of East Asian ETC frequency and genesis regions. ETC frequency in East Asia decrease with an increase of anthropogenic forcing. These declined ETCs are mostly South China

ETCs and are largest in autumn. The reduced ETC frequency seems to be related to an increase of static stability and the decline of vertical zonal wind shear throughout all seasons except winter.

5. Reference

Bengtsson, L., K. I. Hodges, and E. Roeckner, 2006: Storm tracks and climate change. *Journal of Climate*, **19**, 3518-3543.

Chen, S. -J., Y.-H. Kuo, P. -Z. Zhang, and Q. -F. Bai, 1991: Synoptic climatology of cyclogenesis over East Asia, 1958-1987. *Monthly Weather Review*, **119**, 1407-1418.

Chen, S. -J. and P.-Z. Zhang, 1996: Climatology of deep cyclones over Asia and the Northwest Pacific. *Theoretical and Applied Climatology*, **54**, 139-146.

Chung, Y. -S., K. D. Hage, and E. R. Reinelt, 1976: On lee cyclogenesis and airflow in the Canadian Rocky Mountains and the East Asian Mountains. *Monthly Weather Review*, **104**, 879-891.

Colle, B. A., Z. Zhang, K. A. Lombardo, E. Chang, P. Liu, and M. Zhang, 2013: Historical evaluation and future prediction of eastern North American and western Atlantic extratropical cyclones in the CMIP5 models during the cool season. *Journal of Climate*, **26(18)**, 6882-6903.

Dee, D. P., and Coauthors, 2011: The ERA-Interim reanalysis: configuration and performance of the data assimilation system. *Quarterly Journal of the Royal Meteorological Society*, **137**, 553–597.

Eady, E. T., 1949: Long waves and cyclone waves. *Tellus*, **1**, 33-52.

Fink, A. H., T. Brücher, V. Ermert, A. Krüger, and J. G. Pinto, 2009: The European storm Kyrill in January 2007: synoptic evolution, meteorological impacts and some considerations with respect to climate change. *Natural Hazards and Earth System Sciences*, **9(2)**, 405-423.

Graham, N. E. and H. F. Diaz, 2001: Evidence for intensification of North

Pacific winter cyclones since 1948. *Bulletin of the American Meteorological Society*, **82**, 1869-1893.

Gulev, S. K., O. Zolina, and S. Grigoriev, 2001: Extratropical cyclone variability in the Northern Hemisphere winter from the NCEP/NCAR reanalysis data. *Climate Dynamics*, **17(10)**, 795-809.

Hawcroft, M. K., L. C. Shaffrey, K. I. Hodges, and H. F. Dacre, 2012: How much Northern Hemisphere precipitation is associated with extratropical cyclones?. *Geophysical Research Letters*, **39(24)**.

Hayasaki, M. and R. Kawamura, 2012: Cyclone activities in heavy rainfall episodes in Japan during spring season. *SOLA*, **8**, 45-48.

Hayasaki, M., R. Kawamura, M. Mori, and M. Watanabe, 2013: Response of extratropical cyclone activity to the Kuroshio large meander in northern winter. *Geophysical Research Letters*, **40**, 2851-2855.

Hirata, H., R. Kawamura, M. Kato, and T. Shinoda, 2015: Influential Role of Moisture Supply from the Kuroshio/Kuroshio Extension in the Rapid Development of an Extratropical Cyclone. *Monthly Weather Review*, **143**, 4126-4144.

Hodges, K. I., 1994: A general-method for tracking analysis and its application to meteorological data. Monthly Weather Review, 122, 2573-2586.

Hodges, K. I., 1995: Feature tracking on the unit sphere. *Monthly Weather Review*, **123**, 3458-3465.

Hodges, K. I., 1999: Adaptive constraints for feature tracking. *Monthly Weather Review*, **127**, 1362-1373.

Hoskins, B. J. and K. I. Hodges, 2002: New perspectives on the Northern

Hemisphere winter storm tracks. *Journal of the Atmospheric Sciences*, **59**, 1041-1061.

Lambert, S. J., 1996: Intense extratropical Northern Hemisphere winter cyclone events: 1899–1991. *Journal of Geophysical Research: Atmospheres*, **101**, 21319-21325.

Lambert, S. J., and J. C. Fyfe, 2006: Changes in winter cyclone frequencies and strengths simulated in enhanced greenhouse warming experiments: results from the models participating in the IPCC diagnostic exercise. *Climate Dynamics*, **26(7-8)**, 713-728.

Lee, J., J. Kim, and S. -W. Son, 2016: Climatic Features of Extratropical Cyclones During the Spring-time Yellow Dust Events in Korea (in korean). *Atmosphere*, **26**, 565-576.

Nakamura, H., 1992: Midwinter suppression of baroclinic wave activity in the Pacific. *Journal of the Atmospheric Sciences*, **49**, 1629-1642.

Plante, M., S. -W. Son, E. Atallah, J. R. Gyakum, and K. M. Grise, 2014: Extratropical cyclone climatology across eastern Canada. *International Journal of Climatology*, **35**, 2759-2776.

Raible, C. C., 2007: On the relation between extremes of midlatitude cyclones and the atmospheric circulation using ERA40. *Geophysical research letters*, **34(7)**.

Taylor, K. E., R. J. Stouffer, and G. A. Meehl, 2012: An overview of CMIP5 and the experiment design. *Bulletin of the American Meteorological Society*, **93(4)**, 485-498.

Ulbrich, U., J. G. Pinto, H. Kupfer, G. C. Leckebusch, T. Spangehl, and M.

Reyers, 2008: Changing Northern Hemisphere storm tracks in an ensemble of IPCC climate change simulations. *Journal of climate*, **21(8)**, 1669-1679.

Whittaker, L. M. and L. H. Horn, 1984: Northern Hemisphere extratropical cyclone activity for four mid-season months. *International Journal of Climatology*, **4**, 297-310.

Zappa, G., M. K. Hawcroft, L. Shaffrey, E. Black, and D. J. Brayshaw, 2015: Extratropical cyclones and the projected decline of winter Mediterranean precipitation in the CMIP5 models. *Climate Dynamics*, **45(7-8)**, 1727-1738.

Zappa, G., L. C. Shaffrey, K. I. Hodges, P. G. Sansom, and D. B. Stephenson, 2013: A multimodel assessment of future projections of North Atlantic and European extratropical cyclones in the CMIP5 climate models. *Journal of Climate*, **26(16)**, 5846-5862.

Zhang, Y., Y. Ding, and Q. Li, 2012: A climatology of extratropical cyclones over East Asia during 1958–2001. *Acta Meteorologica Sinica*, **26**, 261-277.

6. Figures
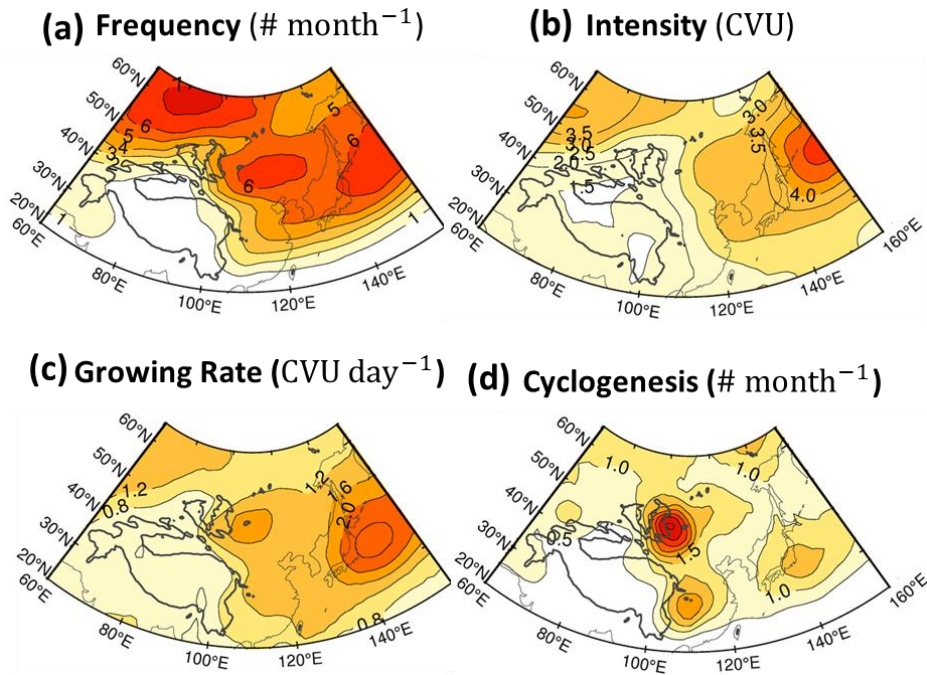
Figure 1. Climatology of extratropical cyclones over the East Asia. Shown are (a) frequency (in number of events per month), (b) intensity (in CVU), (c) growing rate (in CVU per day), and (d) cyclogenesis points (in number of events per month). Thick black lines over continents indicate 2 km high topography.
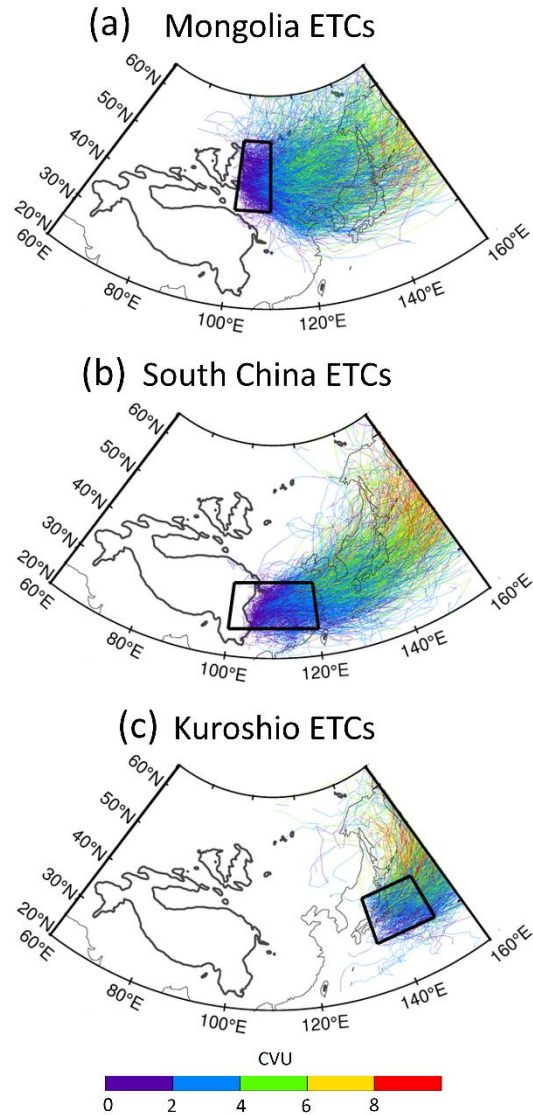
Figure 2. Tracks of extratropical cyclones which generated from the lee side of Altai-Sayan mountain (a), Tibetan Plateau (b), the east sea of Japan (c) in East Asia. Color indicates intensity (in CVU) of extratropical cyclones. Black box represents genesis region of extratropical cyclones.
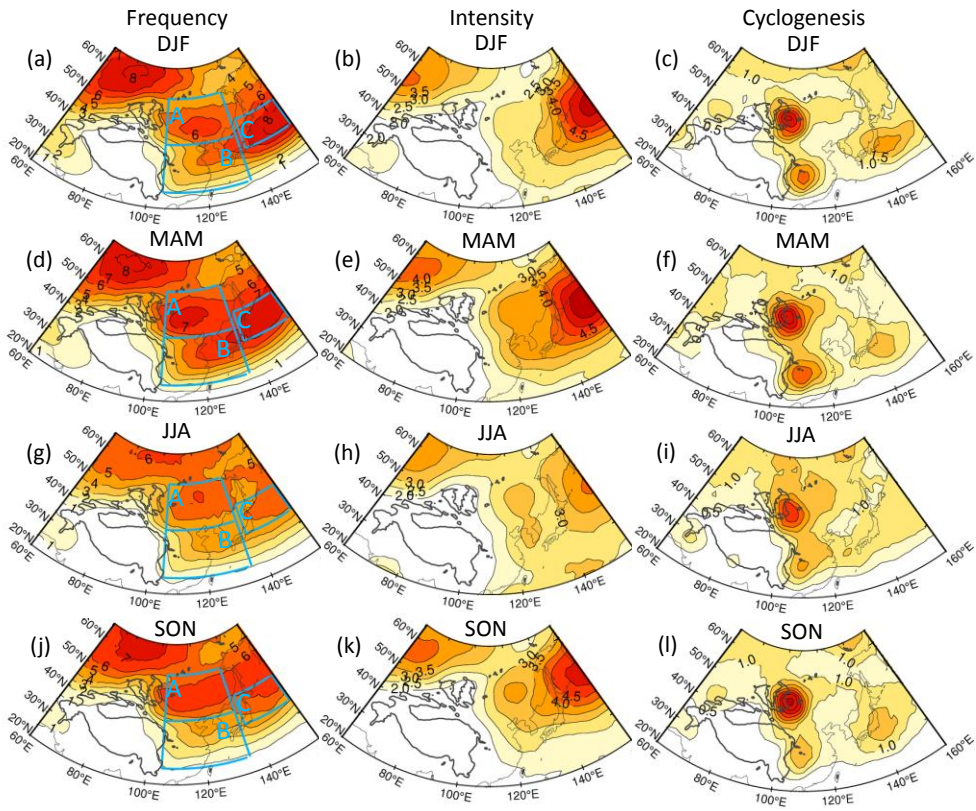
Figure 3. Same as Figs. 2a, b, and d but for (first) winter, (second) spring, (third) summer, and (fourth) autumn.

.
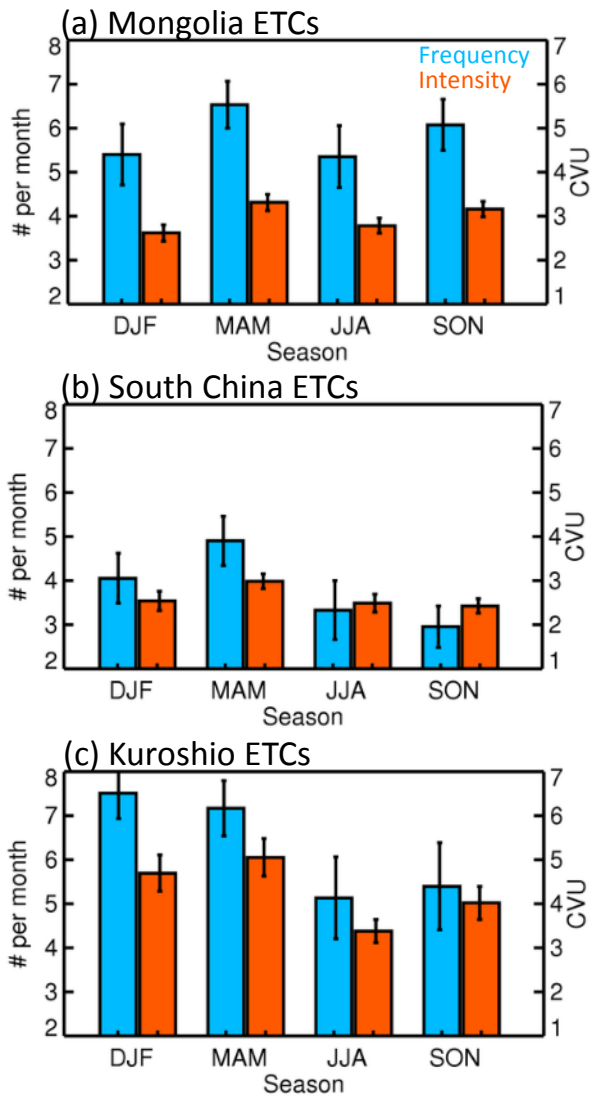
Figure 4. Seasonal cycle of ETC frequency (blue bars) and intensity (orange bars) in the three cyclogenesis regions shown in Fig. 2a. The error bar indicates the interannual variation at one standard deviation.
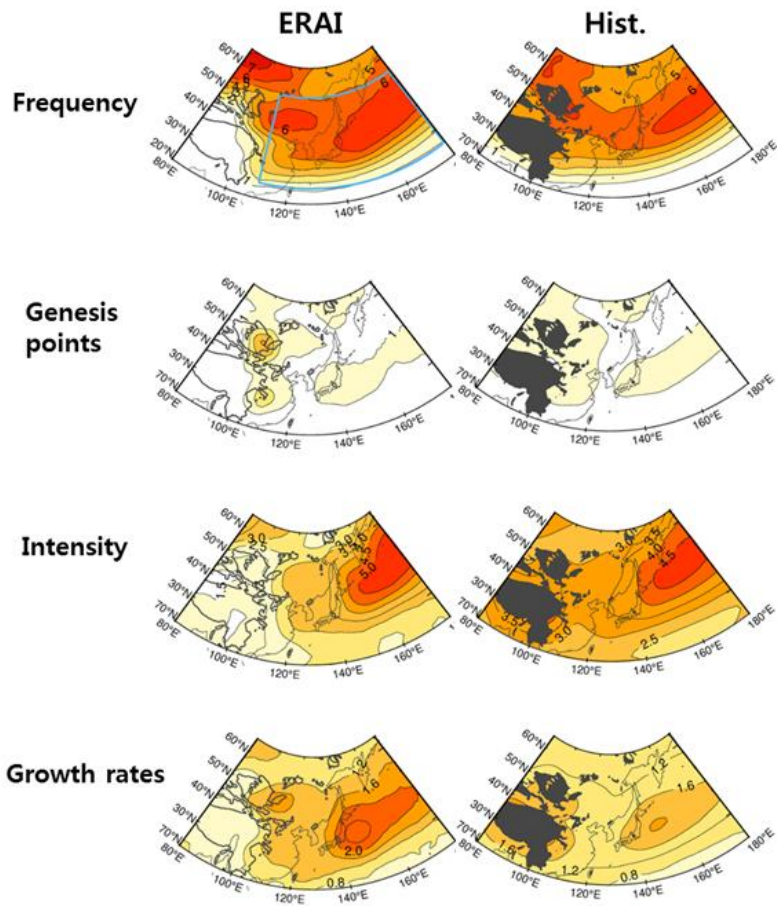
Figure 5. Annual (first) frequency, (second) genesis region, (third) intensity, and (fourth row) growing rates of East Asian extratropical cyclones in (left) ERA-Interim and (right column) historical simulation from 1979 to 2014.
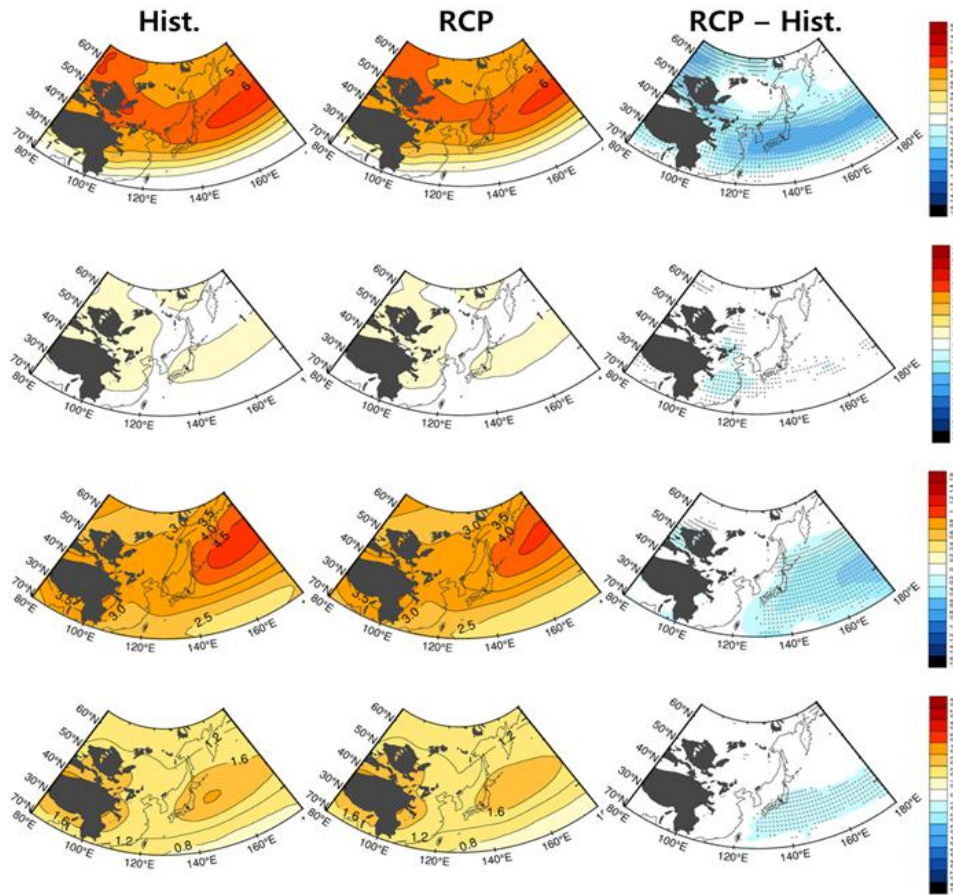
Figure 6. Same as Fig. 5 but for CMIP5 models in (left) historical simulation for 1979-2004, (middle) RCP8.5 scenario for 2074-2099, and for (right column) their response to the RCP8.5 scenario.
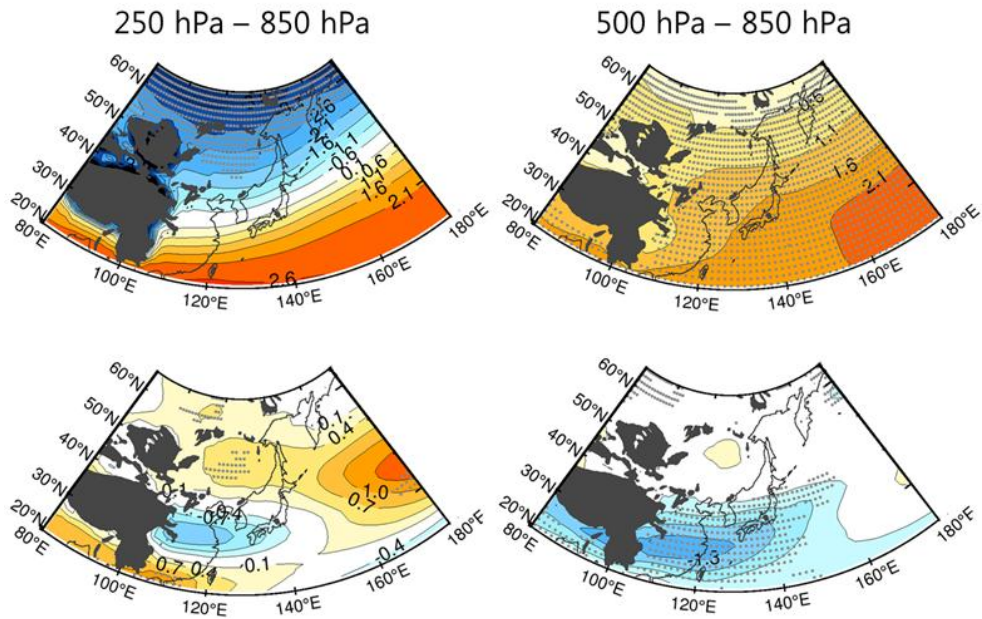
Figure 7. The difference between historical simulation and RCP8.5 scenario for (top) static stability and (bottom row) vertical zonal wind shear. The left (right) column is calculated by the values at 250 hPa (500 hPa) and 850 hPa. Gray dot indicates where more than 80% of CMIP5 models have a difference of same sign.
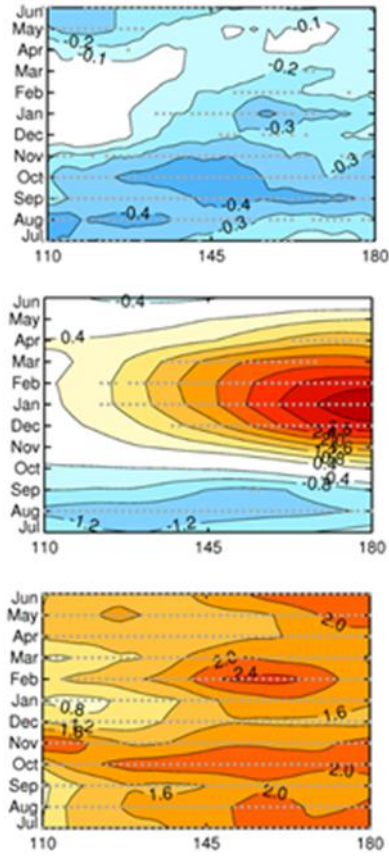
Figure 8. The difference between historical simulation and RCP8.5 scenario for (top) frequency, (middle) static stability and (bottom row) vertical zonal wind shear. Gray dot indicates where more than 80% of CMIP5 models have a difference of same sign.
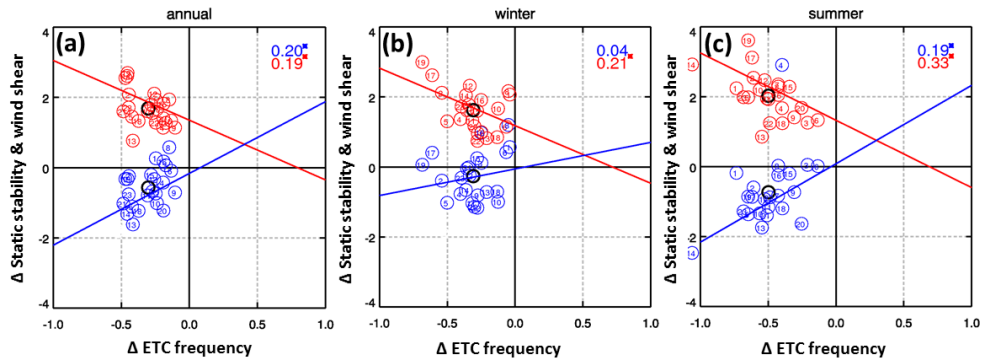
Figure 9. The scatterplots are shown the relationship between (blue/red) cyclone frequency and vertical zonal wind/static stability in annual (left), winter (middle), and summer (right). Dots indicate the results of the individual CMIP5 models. The numbers in upper-right corner present correlation coefficients of their relationships and the asterisk means a significant value..

초   록

CMIP5 모형들에서 나타난 동아시아 온대저기압의 미래 변화

이재연
지구환경과학부
석사과정
서울대학교

본   연구에서   온대저기압은   850   hPa   기압고도의
상대와도장에서 정의되었으며 자동화된 추적 알고리즘을 통해서
탐지   및   추적되었다.   동아시아   온대저기압은   몽골,   남중국,
쿠로시오 해류 지역에서 가장 빈번하게 발생하였다. 이 중에서
몽골   저기압과   남중국   저기압은   풍하측저기압발달에   의해서
발생하는   대륙성   저기압이고   쿠로시오   저기압은   쿠로시오−
오야시오 확장대에서 강한 해수면 경도에 의해 유발되는 경압성에
의해서 발생한다. 미래 동아시아 온대저기압의 변화를 분석하기
위해서 CMIP5 기후 모형들의 historical 모의 실험과 RCP 8.5
시나리오을 비교 분석하였다. CMIP5 기후 모형들은 동아시아
저기압의   발생,   빈도수,   강도,   성장률에   대해서   정량적으로
과소모의하였으나 정성적으로는 그 분포를 잘 모의하였다. 미래

동아시아 온대저기압은 그 수와 강도가 약해지며 이러한 변화는 북서태평양 지역에서 가장 두드러진다. 빈도수의 감소는 남중국과 쿠로시오 해류 지역에서의 온대저기압 발생의 감소와 관련이 있다. 또한 미래 기후에서의 동아시아 온대저기압의 성장 및 발달의 감소는 수직 바람 시어와 정적 안정도의 변화와 관련이 있는 것으로 확인되었다.